SEVENTH EUROPEAN ROTORCRAFT AND POWERED LIFT AIRCRAFT FORUM

Paper No. 42

A NUMERICAL APPROACH TO CO-AXIAL ROTOR AERODYNAMICS

Shigeru Saito
and
Akira Azuma

University of Tokyo
Tokyo, Japan

September 8 - 11, 1981

Garmisch-Partenkirchen
Federal Republic of Germany

Deutsche Gesellschaft für Luft- und Raumfahrt e. V.
Goethstr. 10, D-5000 Köln 51, F.R.G.

A NUMERICAL APPROACH TO CO-AXIAL ROTOR AERODYNAMICS

By

Shigeru Saito and Akira Azuma
Institute of Interdisciplinary Research
Faculty of Engineering
University of Tokyo
Tokyo 153, Japan

ABSTRACT

In the simple momentum theory, the aerodynamic characteristics of the lower rotor of a co-axial rotor system are usually evaluated under the highly deteriorated conditions caused by the fully developed wake of the upper rotor, specifically under the conditions of hovering flight. Analysis using the Local Momentum Theory not only shows the performance of the lower rotor to be higher than that calculated by the simple momentum theory but also makes it possible to calculate the instantaneous airloading of blades operating in a complex wake system. By introducing the radial shrinkage of the rotor wake, the accuracy of the analysis of blade airloading is further improved.

Comparison of the calculated results with those of wind tunnel tests in both hovering and forward flights show good coincidence. In forward flight, the performance of the lower rotor improves not only with increase in the forward speed but also with increase in the vertical distance between the upper and lower rotors. In hovering flight, the improvement in the performance is not remarkable because the lower rotor is strongly influenced by the upper rotor wake.

NOMENCLATURE

A	coefficient in equation (2)
a	lift slope
b	number of blades
C	attenuation coefficient
C_T	thrust coefficient = $T/\rho(\pi R^2)(R\Omega)^2$
C_Q	torque coefficient = $Q/\rho(\pi R^2)(R\Omega)^2 R$
c	blade chord
d	rotor clearance between upper and lower rotors
i_s	rotor shaft angle

k_1, k_2	coefficients in equation (1)
ℓ	airloading along blade span
Q	torque
q	blade section torque
R	rotor radius
r	spanwise position on blade
r_T	position of tip vortex in radial direction in equation (2)
T	thrust
t	time
V	forward velocity
v	induced velocity
v_z	axial transport velocity in equation (7)
x	nondimensional spanwise position = r/R
z	radial position
z_T	position of tip vortex in axial direction in equation (1)
Γ	circulation of tip vortex
Δ	small increment
θ	blade pitch angle (positive leading-edge up) $= \theta_0 + \theta_t(x - 0.75) + \theta_{1c}\cos\psi + \theta_{1s}\sin\psi + \cdots$
θ_0	collective pitch angle
θ_t	blade twist angle
λ	inflow ratio = $(V\sin i_s + v)/R\Omega$
λ_T	coefficient of wake contraction in equation (2)
μ	advance ratio = $V\cos i_s/R\Omega$
ρ	air density
σ	solidity = $bc/\pi R$
χ	wake skew angle = $\tan^{-1}(\lambda/\mu)$
ψ	azimuth angle, clockwise for upper rotor and counter-clockwise for lower rotor
ψ_w	azimuth angle of tip vortex in equation (2)
Ω	rotor rotational speed

Subscripts:

(ℓ, m)	coordinate of station on rotational plane
m	mean value
T	tip vortex
1	lower rotor
2	upper rotor

1. INTRODUCTION

Several wake models have been proposed for evaluating the induced velocity distribution along a blade span. They are (i) simple momentum theory [1, 2], (ii) Fourier series presentation [3], (iii) local momentum theory (LMT) [4], (iv) vortex theories with prescribed wake [5, 6, 7] and free wake [1]. Among these methods, (i), (ii) are useful for overall estimation of performance, and (iv) are more vigorous methods than the others but have the shortcoming of requiring considerable computation time. On the other hand, (iii) is more divergence free and saves computation time. This theory (LMT) is based on the instantaneous balance between the fluid momentum and the blade elemental lift at a local station in the rotor rotational plane. Therefore the theory has the capability of evaluating timewise variations of airloading, aerodynamic moments and induced velocity distributions along the blade span. The theory has been applied successfully to many problems of helicopter rotors [8, 9, 10].

Although there is a vast amount of literature dealing with single rotors, there have to date been few papers concerning multi-rotor systems. For a co-axial rotor system, theoretical predictions have been conducted using the vortex-strip theory [11] and experimental studies have also been carried out to evaluate the optimal performance for a co-axial rotor [12 ∿ 15] and for an Advancing Blade Concept (ABC) rotor [16 ∿ 20]. It has been found from these studies that in both hovering and forward flights the co-axial rotor system can have more blade loading than an equivalent single rotor at the same torque level.

The purpose of this paper is to investigate the aerodynamic characteristics of a co-axial rotor system in both hovering and forward flights, and to verify the validity of the present method based on the generalized wake model in hovering flight by applying the LMT to such phenomena. The theoretical results were compared with wind tunnel test data and showed reasonable agreement with them.

The authors wish to thank Professor T. Nagashima for his kind presentation of wind tunnel test data on co-axial rotor systems and for his advice on the calculated results. Further thanks are extended to Dr. K. Kawachi for his suggestion to apply his computational method for single rotor hover performance to the calculation of co-axial rotor performance.

2. ROTOR WAKE GEOMETRY

In hovering flight, wake contraction plays an important role in the estimation of rotor performance. A theoretical prediction not using a contracted wake model becomes increasingly inaccurate as the rotor solidity, the thrust level, and the tip Mach number increase. The vortex theory based on the free wake model includes these effects on the rotor performance but as mentioned in the preceding section it has inherent difficulties in computing technique. The vortex theory with prescribed wake model can overcome these shortcomings, but it requires advance knowledge of wake geometry to predict the aerodynamic characteristics.

Landgrebe et al. [21~24] have performed experimental tests to determine the wake geometry for single rotors with configurational parameters in hovering flight by using a high-speed-photograph technique. They have derived a generalized wake geometry from the experiments as follows:

$$Z_T/R = \begin{cases} k_1\psi_w & 0 \leq \psi_w \leq (2\pi/b) \\ k_1(\frac{2\pi}{b}) + k_2(\psi_w - (\frac{2\pi}{b})) & \psi_w \geq (2\pi/b) \end{cases} \tag{1}$$

$$r_T/R = A + (1 - A)e^{-\lambda_T\psi_w} , \tag{2}$$

where

$$
\begin{aligned}
A &= 0.78 \quad \text{(near-wake)} \\
k_1 &= 0.25(C_T/\rho + 0.001\theta_t) \\
k_2 &= (1.41 + 0.0141\theta_t)\sqrt{C_T/\rho} \\
\lambda_T &= 0.145 + 27C_T \ ,
\end{aligned}
\tag{3}
$$

and where (r_T, ψ_W, z_T) is the spatial position (radial, azimuth angle, and axial position) of a tip vortex in the stable near-wake region.

Kocurek and Tangler[25] have also conducted experiments to re-estimate the generalized wake geometry which was derived by Landgrebe et al. using the schilieren photograph technique. They have derived the same generalized wake geometry but with a little different expression of the parameters k_1 and k_2. In the subsequent calculation, the Landgrebe model will be used.

Nagashima et al. [13,15] have conducted experiments by means of the flow visualization method to estimate the trajectories of the tip vortices shed from each rotor of a co-axial rotor system in hovering flight. Their results show that under appropriate conditions, i.e. specific combinations of rotor vertical spacing and collective pitch angle, the performance of a co-axial rotor is improved. Fig. 1 a, b and c are examples of flow visualization which show the trajectories of the tip vortices of different rotors [13]. Fig. 2 a, b and c show the spatial position of tip vortices in the (r_T, z_T) vs ψ_W plane. In this figure, the experimental data are compared with the generalized wake model derived by Landgrebe for a single rotor with the same thrust level. One can derive the conclusion that the tip vortices of each rotor descend more rapidly than those of the equivalent single rotor. Since the upper and lower rotors in a co-axial rotor system are arranged vertically with some clearance, the flow field of one rotor influences the other, specifically the induced velocity of the upper rotor greatly deteriorates the performance of the lower rotor. However, as the lower rotor absorbs the wake of the upper rotor, the tip vortices of the upper rotor move downward more quickly than those of a single rotor. This leads to an improvement in the upper rotor performance, specifically in hovering flight.

In this paper, in consideration of Ref. 13, the generalized wake model in eqs. (1) and (2) has been adopted as the wake model for each rotor of co-axial rotor system and the wake model of the lower rotor has been considered as that of the single rotor in vertical flight at the speed of the mean induced velocity of the upper rotor.

3. WAKE MODEL OF A CO-AXIAL ROTOR SYSTEM

3-1 Wake Model in Hovering Flight

There are many papers which use the vortex theory based on prescribed wake geometry to calculate single rotor hover performance [23, 25]. In Ref. 26, Kawachi has extended the LMT to calculate single rotor hover performance by using the generalized wake model. The results show good coincidence with the experimental data and the theory presented by Landgrebe[22]. In the LMT, the spanwise wake deformation is equivalent to the spanwise movement of a local station on the rotor rotational plane. Fig. 3 (a) and (b) show a side view and a top view of the tip vortices of each rotor. The tip vortex No. 1 in Fig. 3 (a) is shed from the blade (A) at position P_{21} (for the upper rotor) or at position P_{11} (for the lower rotor) at time $t = j$. The tip vortex No. 2 is shed from the blade (B) which preceded the blade (A) at position P_{21} or P_{11} at time $t = j - 1$, and is located at position P_{22} at time $t = j$. The period between $t = j - 1$ and $t = j$ is the time during which two neighboring blades successively pass through the same position of the rotor rotational plane. In a rotor with b blades, that time, Δt, is $2\pi/b\Omega$. During the period Δt, the vortex No. 2 moves from P_{21} to P_{22} for the upper rotor (or from P_{11} to P_{12} for the lower rotor). At the same time it moves from r_{21} to r_{22} (or from r_{11} to r_{12}) along the blade span. Generally, the radial position can be written as r_{mn} for the m th rotor and n th tip vortex. Similarly, each station moves from r_{mn-1} to r_{mn} during the period Δt. In the present calculation, the wake azimuth angle $\psi_{w,n}$ of the tip vortex No. n is given as

$$\psi_{w,n} = (2\pi/b)(n - 1) \ . \tag{4}$$

Outside the rotor disc ($r > R$), each station may be assumed to be a distance ($r_{11} - r_{12}$) toward the blade root whereas at the inner area of the rotor ($r \leq AR$) the station is assumed to remain constantly at its initial position in line with eqs. (1) and (2) for the near-wake.

In the co-axial rotor system, the above assumptions are maintained with minor modification for the coefficients of eq. (1) as follows: In Ref. 23, the constants k_1 and k_2 are defined by

$$k_1 \text{ or } k_2 = \frac{\Delta z_T/R}{\Delta \psi_w} = \frac{v_z}{R\Omega} \tag{5}$$

for $\quad k_1 : \Delta\psi_w = 2\pi/b$

$$\Delta z_r/R = (z_r/R)\psi_w = \psi_w - (z_r/R)\psi_w = 0 \tag{6a}$$

for $\quad k_2 : \Delta\psi_w = \psi_w - 2\pi/b$

$$\Delta z_T/R = (z_T/R)\psi_w = \psi_w - (z_T/R)\psi_w = \frac{2\pi}{b} \ , \tag{6b}$$

where v_z denotes the axial transport velocity of the tip vortex. The induced velocity of the upper rotor may be considered to reach the surface of the lower rotor with the magnitude of $K_{21}v_2$, where K_{21} is the ratio of the developed velocity and the velocity, v_2, just before a blade of the upper rotor has passed. Since the wake shrinks toward the inner area of the lower rotor, $K_{21}v_2$ is not at the same position as that of v_2 in the radial direction. So, in this calculation, the position that the velocity v_2 would reach has been, from eqs. (1) and (2), determined by considering the wake shrinkage as follows:

$$(r_T/R)_{22} = A + (1 - A)e^{-\lambda_T\psi_{w,22}} \tag{7}$$

$$\psi_{w,22} = \{(2\pi/b)(k_2 - k_1) + (d/R)\}/k_2 \tag{8}$$

$$(r_T)_{22} = (r_T/R)_{22} \cdot (r_T)_{21} , \qquad (9)$$

where the constants k_1, k_2 and A can be determined by eqs. (3), and d is the distance between the upper and lower rotors (rotor clearance). Subscript 22 denotes the value when the wake of the upper rotor reaches the surface of the lower rotor. For the upper rotor, the influence of the lower rotor can be determined by the momentum theory as follows:

$$v_{12} = C_{12} v_1 = C_{12} R\Omega\sqrt{C_{T_1}/2} \qquad (10a)$$

$$C_{12} = f_n(d, C_{T_1}) . \qquad (10b)$$

The value of $C_{12}v_1$ is, for example at $d/R = 0.26$, about thirty percent of the mean induced velocity $v_1 = R\Omega\sqrt{C_{T_1}/2}$ according to the simple vortex theory [27]. Then, by assuming that this induced velocity v_{12} uniformly flows into the upper rotor surface, the nondimensional induced velocity of the upper rotor is given as

$$\lambda_2 = \frac{1}{2} \{ (\frac{C_{12} v_1}{R\Omega}) + \sqrt{(\frac{C_{12} v_1}{R\Omega})^2 + 2C_{T_2}} \} . \qquad (11)$$

If C_{12} is zero (single rotor), this yields

$$\lambda_{2m} = \sqrt{C_{T_2}/2} . \qquad (12)$$

Then, the ratio of eqs. (11) and (13) is given by

$$\frac{\lambda_2}{\lambda_{2m}} = \frac{1}{2} \{ C_{12} (\frac{\lambda_1}{\lambda_{2m}}) + \sqrt{C_{12}{}^2 (\frac{\lambda_1}{\lambda_{2m}})^2 + 4} \} \simeq 1 + \frac{C_{12}}{2} (\frac{\lambda_1}{\lambda_{2m}}) . \qquad (13)$$

The value of $\frac{C_{12}}{2} (\frac{\lambda_1}{\lambda_{2m}})$ is several percent for $d/R = 0.26$, and, therefore, the thrust level of the upper rotor becomes higher as the rotor clearance increases, because the coefficient C_{12} decreases appreciably.

The above results derived from the simple momentum theory well reveal why the experimental data [13] tend to deviate from theoretical results based on single rotor analysis (See Fig. 2).

A new model was developed to take the wake deformation into account and to obtain the attenuation coefficient at the upwash region [25, 26, 27]. The new model consists of a vortex ring and a semi-infinite vortex cylinder. The vortex ring represents the tip vortex nearest the rotor rotational plane, and the vortex cylinder represents the remaining tip vortices. The strength of the vortex ring is equal to that of the tip vortex. The strength of the vortex cylinder is equal to that of the axially averaged tip vortices [27]. In hovering flight the tip vortices are very close to the rotor. So in the calculation of the attenuation coefficients the tip vortices of the near region were concentrated as a vortex ring and those of the far region were represented as a vortex cylinder. Fig. 4 (a) shows that the preceding blade (B) passes through a local station at time $t = j - 1$. The vortex ring is located on the rotor rotational plane, and the top of the vortex cylinder is located at the position of the second tip vortex. The distance between the top of the vortex cylinder and the rotor rotational plane is z_{m2}. Fig. 4 (b) shows that following blade (A) comes to a position just before the station at time $t = j$. During this time interval, the two vortex systems move downward and radially contract. The vertical position z_{mn} is determined from the eqs. (1) and (4) as follows:

$$z_{mn} = \begin{cases} Rk_1\psi_{w,n} & n \leq 2 \\ R\{k_1(2\pi/b) + k_2(\psi_{w,n} - (2\pi/b))\} & n > 2 . \end{cases} \tag{14}$$

The radii of the vortex ring and the vortex cylinder during the time between $t = j - 1$ and $t = j$ are given by eqs. (2) and (4). In the LMT, the attenuation coefficient is defined by the changing rate of induced velocities at a station (ℓ, m) on the rotor rotational plane during the time interval concerned. In the new model, the station (ℓ, m) moves from position r_{mn-1} to position r_{mn} on the rotor rotational plane. Therefore, the attenuation coefficient of that station is given as

$$C_{\ell m}^{j-1} = v_{\ell m}^{j}(r = r_{mn})/v_{\ell m}^{j-1}(r = r_{mn-1}). \tag{15}$$

If the vortex cylinder alone is adopted as a wake model to calculate the attenuation coefficients, the induced velocity $v_{\ell m}^{j-1}$ is zero on the rotor plane outside the rotor disc. Therefore it is impossible to define the attenuation coefficients of these stations. Consequently, the discrete vortex mentioned above was introduced into the present model.

In eq. (3), the constants k_1 and k_2 are functions of thrust coefficient. In this paper, the thrust coefficient of the rotor is calculated at each time step and used to determine the constants k_1 and k_2. The calculation is completed when the thrust coefficient reaches a steady state.

3-2 Wake Model in Forward Flight

In forward flight, the wake model may be considered to be as shown in Fig. 5 [8], in which the wake contraction is disregarded for simplicity. The effect of the tip vortex shed from the preceding blade is taken into consideration in the calculation by using the LMT. In this paper the attenuation coefficient may be considered constant all over the rotor disc because (i) counter-rotated rotors will tend to have a homogeneous velocity distribution, (ii) at high advance ratio a constant attenuation coefficient is not so improper in the single rotor and may be similar in the co-axial rotors, and (iii) the saving of computation time and the simplification in programing will be appreciable.

The actual procedure for determining the constant attenuation coefficient is as follows: The induced velocity at a local station on the lower rotor disc, v_1, is given by the summation of the induced velocity generated by the lower rotor itself, v_{11}, and that induced by the upper rotor, v_{21},

$$v_1 = v_{11}(v_1,\ \psi_1;\ t) + v_{21}(r_2,\ \psi_2,\ d;\ t) \tag{16}$$

where t is time and the other symbols are as shown in Fig. 5. The induced velocity v_{21} is given by multiplying the attenuation coefficient of the upper rotor by the mean induced velocity of the same rotor,

$$v_{21} = v_2 C_{21}(\chi_2,\ z_2,\ d) \tag{17}$$

where

$$C_{21}(\chi_2,\ z_2,\ d) = (v_2/v_{0,2})_1\ . \tag{18}$$

Similarly, the induced velocity of any local station on the upper rotor disc is given by

$$v_2 = v_{22}(r_2,\ \psi_2;\ t) + v_{12}(r_1,\ \psi_1,\ d;\ t) \tag{19}$$

where

$$v_{12} = v_1 C_{12}(\chi_1,\ z_1,\ d) \tag{20a}$$

$$C_{12} = (v_1/v_{0,1})_2\ . \tag{20b}$$

Since C_{12} is smaller than C_{21}, the following approximation is allowable:

$$v_2 \simeq v_{22}\ , \quad v_{12} \simeq 0\ . \tag{21}$$

The attenuation coefficients of the two rotors are given respectively by

$$C_1 = v_1/v_{0,1} \tag{22a}$$

$$C_2 = v_2/v_{0,2}\ . \tag{22b}$$

These attenuation coefficients are under some operational conditions calculated by the interation method using the wake model shown in Fig. 5.

4. CALCULATION RESULTS

Numerical calculations have been conducted to verify the validity of the present method for a co-axial rotor system. The calculated results were compared with the experimental data in hovering flight [14] and in forward flight [12]. Table 1 shows the geometrical characteristics and the operating conditions used in these calculations.

4-1 Hovering Flight

The theoretical calculations using the generalized wake model were performed for a co-axial rotor in hovering flight.

Fig. 6 shows the performance curves of the upper and lower rotors of a co-axial rotor in hovering flight together with the experimental data. The calculated results are in good coincidence with the experimental data. Fig. 7 shows the total performance of the co-axial rotor system, together with the equivalent single rotor performance with two and four blades. In this figure, the performance of the single rotor is compared with that of the co-axial rotor in blade loading C_T/σ vs blade torque C_Q/σ plane. The solidity of the single rotor is 0.1 for the two bladed rotor and is 0.2 for the four bladed one. It is found that the performance of a co-axial rotor is inferior to the two bladed single rotor but is slightly superior to the four bladed single rotor.

Fig. 8 shows lift distributions along the blade span for several pitch angles, in which the solid lines denote the lift distribution for the lower rotor and dotted lines denote that for the upper rotor. In the upper rotor, the lift is positive everywhere along whole span and a peak in the lift caused by the wake contraction is observed near the blade tip. On the contrary, in the lower rotor negative lifts are generated near the rotor root. This tendency is more pronounced when the collective pitch angle of the lower rotor is small. Since the lower rotor operates in the wake of the upper rotor, all sections of a blade are affected by the induced velocity from the tip vortex wake of the upper rotor.

In Fig. 9, the effect of the blade twisted angle on the co-axial rotor performance is shown. It is found that the performance is slightly improved by the blade twist. The reason is that the lift distributions at the inner part of the rotor are improved by setting a blade twist.

Fig. 10 shows the spanwise induced velocity distribution along a blade span. The induced velocities at the inner part of the lower rotor are about twice those of the upper rotor. At about the 70 percent radius position on the blade span, the induced velocity once dips and gradually recovers toward the tip of the blade. The dip results from the fact that the accelerated downwash velocity of the upper rotor reaches the lower rotor blade with contraction, and the outer part of the blade (near the tip) operates in the upwash velocity field of the upper rotor. In the upper rotor, the induced flow pattern is different from that of the lower one and the effect of the wake contraction is seen at the 80 $\sim$ 90 percent spanwise position. It is found from these results that the bending moment of the lower rotor blade is strongly influenced by the downwash distribution on the lower rotor, specifically at the inner part of the rotor.

Shown in Fig. 11 is the spanwise torque distributions along the blade spans of the upper and lower rotors. Similarly to the lift distributions, the torque distributions at the inner part of the blade span are strongly influenced by the downwash velocities of the upper rotor.

4-2 Forward Flight

Performance calculations for a co-axial rotor in forward flights were conducted and the results were compared with experimental data. Fig. 12 shows the performance curves of a co-axial rotor system flying with a specified advance ratio of μ = 0.16 for various rotor clearances d. As the clearance increases, the performance moves away from that of a four bladed single rotor having twice the solidity and approaches that of a two bladed single rotor. The discrepancy in the polar curve at d/R = 0.21 seems to be the result of disregarding the wake contraction.

Shown in Fig. 13 are the theoretical calculation and the wind tunnel test results for the performance of a co-axial rotor model having a vertical distance of d = 0.24 m or d/R = 0.63. As the advance ratio increases, the thrust coefficient increases and torque coefficient decreases. These figures are reproductions from figure 14 and 13 respectively in Ref. 8.

Fig. 14 shows blade loadings vs advance ratio at d/R = 0.42 and the same collective pitch angle, $\theta_{01} = \theta_{02} = 9^\circ$, for both rotors. The results by simple vortex theory [12] are shown together in the same figure. A difference between the results by the LMT and the experimental data apprears at $\mu = 0.12$. This may be due to the assumption that the attenuation is constant all over the rotor disc.

In Fig. 15, the effects of the vertical rotor clearance on the blade loading are shown together with the experimental results and the results of the vortex theory. As the rotor clearance becomes larger, the performance of the lower rotor is improved because of the decrease in the disturbed area on the lower rotor. The results are in good coincidence with the experimental data.

Fig. 16 shows the lift distribution along a blade span at azimuth angle $\psi = 0^\circ$ and $\psi = 180^\circ$ in forward flight. From this figure it is found that the performance of the rotors is nearly equal. The downwash distributions along the longitudinal axis through the hub at the same flight condition are shown in Fig. 17. The magnitude of this downwash distribution for the upper rotor is slightly larger than that for the lower one at the fore part of the rotor. However, there is no difference in the total performance of the two rotors [see Fig. 13]. Since in forward flight the wake of each rotor moves away from the rotor to the rear, the influence of each wake on the other rotor becomes weak.

5. CONCLUSION

The Local Momentum Theory was applied to co-axial rotor performance calculation in both hovering and forward flights. The calculated results were compared with wind tunnel test data and the results of other theories and shown to be in good agreement. The following conclusions were reached:

In hovering flight

1) The performance of the co-axial rotor is slightly better than that of an equivalent single rotor (same blade loading). Furthermore, the power of the co-axial rotor is about 8% lower than that of an equivalent single rotor for the same operating conditions.

2) The performance of the lower rotor is only slightly improved by increasing the rotor clearance. Increasing the rotor clearance has rather a greater effect toward improving the flow pattern of the upper rotor.

3) The setting of a blade twisted angle θ_t, usually negative, improves the performance of the co-axial rotor.

4) By using the generalized wake model modified for the co-axial rotor system, the LMT can be applied to estimation of co-axial rotor performance.

5) In these calculations solutions in convergent state can be obtained in about 20 seconds using a FACOM M-200 computer.

In forward flight

1) As the rotor clearance d increases, the performance of the lower rotor improves dramatically and approaches that of a single rotor.

2) The lower rotor behaves as a single rotor at high forward speed for any rotor clearance.

3) The assumption that the attenuation coefficient is constant all over the rotor disc is valid for the co-axial rotor system in forward flight, except at low advance ratio.

4) The computation time required to obtain a steady state solution by the present method is about 80 seconds.

REFERENCES

1. Johnson, W.: "Helicopter Theory." Princeton University Press, 1980.

2. Stepniewski, W. Z.: "Introduction to Helicopter Aerodynamics." Rotary Aircraft Series, No. 3, Rotorcraft Publishing Committee, Morton, PA., 2nd Printing, 1958.

3. Miller, R. H.: "Rotor Blade Harmonic Airloading." AIAA Journal, Vol. 2, No. 7, July, 1964.

4. Azuma, A. and Kawachi, K.: "Local Momentum Theory and Its Application to the Rotary Wing." Journal of Aircraft, Vol. 16, No. 1, January, 1979.

5. Biggers, J. C., Lee, A., Orloff, K. L. and Lemmer, O. J.: "Measurements of Helicopter Rotor Tip Vortices." The 33rd Annual National Forum of the AHS, Preprint 77.33-06, May, 1977.

6. Samant, S. S. and Gray, R. B.: "A Semi-Empirical Correction for the Vortex Core Effect on Hovering Rotor Wake Geometries." The 33rd Annual National Forum of the AHS, Preprint No. 77.33-02, May, 1977.

7. Summa, J. M. and Maskew, B.: "New Methods for the Calculation of Hover Airloads." The Fifth European Rotorcraft and Powered Lift Aircraft Forum, Paper No. 15, Sept. 4-7, 1979.

8. Azuma, A., Saito, S., Kawachi, K. and Karasudani, T.: "Application of the Local Momentum Theory to the Aerodynamic Characteristics of Multi-Rotor Systems." Vertica, Vol. 3, No. 2, 1979.

9. Azuma, A. and Saito, S.: "Study of Rotor Gust Response by Means of the Local Momentum Theory." Paper No. 27, The Fifth European Rotorcraft and Powered Lift Aircraft Forum, Sept. 4-7, 1979.

10. Saito, S. Azuma, A. and Nagao, M.: "Gust Response of Rotary Wing Aircraft and Its Alleviation." Vertica, Vol. 5, No. 2, pp.173 - 184, 1981.

11. Andrew, M. J.: "Co-Axial Rotor Aerodynamics in Hover." Vertica, Vol. 5, No. 2, pp.163 - 172, 1981.

12. Shinohara, K.: "Wind Tunnel Test on the Performance of a Co-Axial Rotor." A Graduation Thesis, Department of Aeronautics, 1977, in Japanese.

13. Nagashima, T., Shinohara, K. and Baba, T.: "A Flow Visualization Study for the Tip Vortex Geometry of the Co-Axial Rotor in Hover." J. of Japan Society for Aeronautics and Space Science, Vol. 25, No. 284, Sept., 1977, in Japanese.

14. Nagashima, T., Ōuchi, H. and Sasaki, F.: "Optimum Performance and Load Shearing of Co-Axial Rotor in Hover." J. of Japan Society for Aeronautics and Space Sciences, Vol. 26, No. 293, June, 1978, in Japanese.

15. Nagashima, T. and Nakanishi, K.: "Optimum Performance and Wake Geometry of Co-Axial Rotor in Hover." The Seventh European Rotorcraft and Powered Lift Aircraft Forum, Paper No. 41, Sept. 8-11, 1981.

16. Burgess, R. K.: "Development of the ABC Rotor." The 27th Annual National V/STOL Forum of the AHS, Preprint No. 504, May, 1971.

17. Halley, D. H.: "ABC Helicopter Stability, Control, and Vibration Evaluation on the Princeton Dynamic Model Track." The 29th Annual National Forum of the AHS, Preprint No. 744, May, 1973.

18. Abbe, J. T. L., Blackwell, R. H. and Jenney, D. S.: "Advancing Blade Concept (ABC)™ Dynamics." The 33rd Annual National Forum of the AHS, Preprint No. 77.33-31, May, 1977.

19. Cheney, M. C., Jr.: "The ABC Helicopter." AIAA/AHS VTOL Research, Design, and Operations Meeting, AIAA, Paper No. 69-217, Feb. 17-19, 1969.

20. Ruddell, A. J.: "Advancing Blade Concept (ABC™) Development." The 32nd Annual National V/STOL Forum of the AHS, Preprint No. 1012, May, 1976.

21. Jemey, D. S., Olson, J. R. and Landgrebe, A. J.: "A Reassessment of Rotor Hovering Performance Prediction Methods." The 23rd Annual National Forum of the AHS, Preprint No. 100, May, 1967.

22. Landgrebe, A. J.: "An Analytical and Experimental Investigation of Helicopter Rotor Hover Performance and Wake Geometry Characteristics." USAAMRDL TR 71-24, Eustis Directorates, U. S. Army Air Mobility Research and Development Laboratory, Ft. Eustis, Virginia, June, 1971.

23. Landgrebe, A. J.: "The Wake Geometry of a Hovering Helicopter Rotor and its Influence on Rotor Performance." J. of the AHS, Vol. 17, No. 2, Oct. 1972.

24. Landgrebe, A. J. and Bellinger, E. D.: "Experimental Investigation of Model Variable Geometry and Oge Tip Rotors." The 29th Annual National Forum of the AHS, Preprint No. 703, May, 1973.

25. Kocurek, J. D. and Taugler, J. L.: "A Prescribed Wake Lifting Surface Hover Performance Analysis." J. of the AHS, Vol. 22, No. 1, Jan., 1977.

26. Kawachi, K.: "An Extension of the Local Momentum Theory to a Distorted Wake Model of a Hovering Rotor." NASA TM 81258, Feb., 1981.

27. Castles, W., Jr., and De Leeuw, J. H.: The Normal Component of the Induced Velocities in the Vicinity of a Lifting Rotor and Some Examples of Its Application." NASA Report 1184, 1954, (supersedes NACA TN 2912).

Table I Rotor Dimensions

Items		Dimensions	
Rotor radius,	R	0.38	m
Blade chord,	c	0.06	m
Blade cutoff,	r_c	0.08	m
Position of flapping hinge,	r_β	0.037	m
Angle of rotor shaft,	i_s	0	deg
Lift slope,	a	5.3	
Number of blades,	b	2 or 4	
Blade mass,	m_β	0.0051	$\mathrm{Kg\text{-}sec^2/m}$
Rotor rotational speed,	Ω	324.6	rad/sec
Blade twist,	θt	$0^\circ, -6^\circ$	deg
Moment of inertia,	I_β	$2.0337\mathrm{x}10^{-4}$	$\mathrm{Kg\text{-}m/sec^2}$
Drag coefficient of blade section,	c_{d_0}	$\delta_0 = 0.0148$	
$c_{d_0} = \delta_0 + \delta_1 \alpha_r + \delta_2 \alpha_r^2$		$\delta_1 = -0.048$	
		$\delta_2 = 1.48$	
Solidity,	σ	0.1 (b=2)	
		0.2 (b=4)	
Rotor spacing,	d	0.08-0.24	m

(a) (b) (c)

(a) SINGLE ROTOR
$\theta_0 = 9^\circ$

(b) CO-AXIAL ROTOR
$(\theta_{02}, \theta_{01}) = (9^\circ, 10^\circ)$, $d/R = 0.42$

(c) CO-AXIAL ROTOR
$(\theta_{02}, \theta_{01}) = (9^\circ, 10^\circ)$, $d/R = 0.63$

13)

Figure 1. Examples of flow visualization.

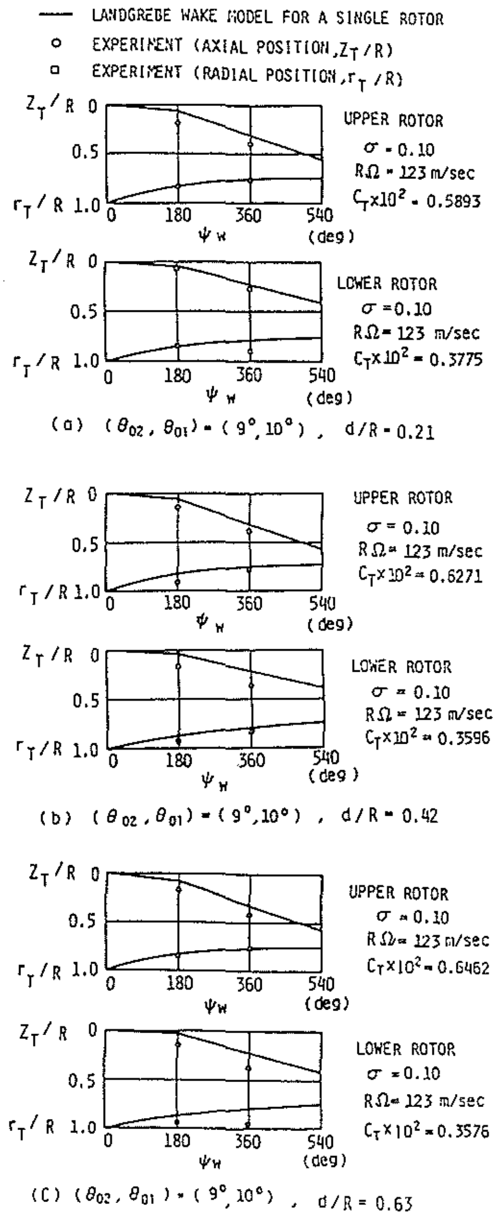

13)

Figure 2. Spacial disposition of tip vortices in co-axial rotor.

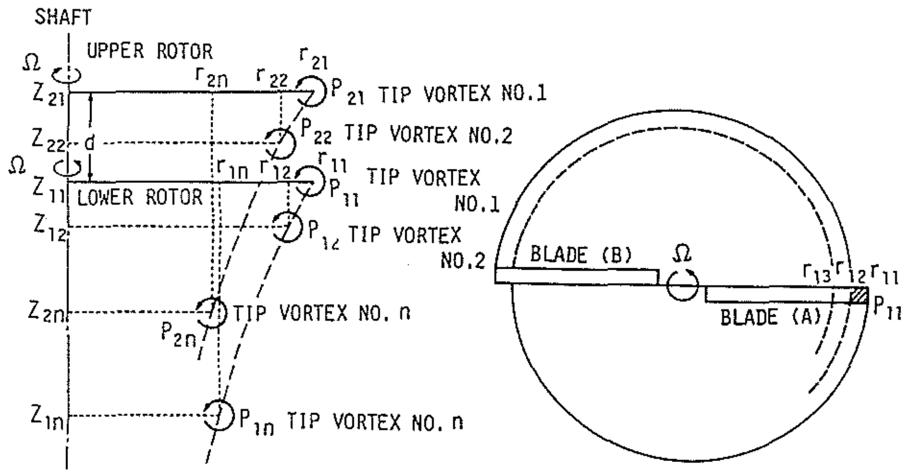

(a) SIDE VIEW OF TIP VORTICES IN MODEL. (b) TOP VIEW OF TIP VORTICES OF THE UPPER ROTOR IN MODEL.

Figure 3. Views of tip vortices.

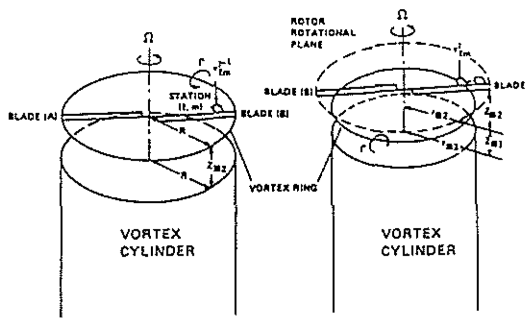

(a) $t = j - 1$ (b) $t = j$

Figure 4. Extended model for attenuation coefficient.

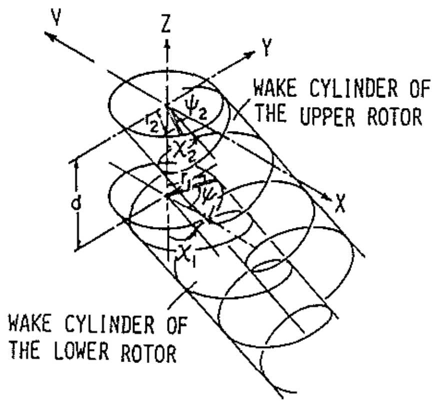

Figure 5. Coordinate systems of coaxial rotor system.

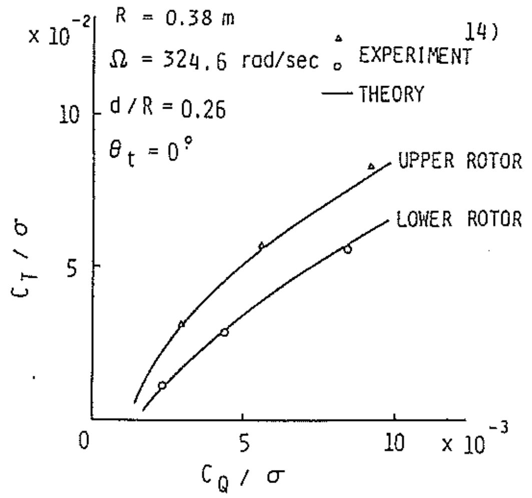

Figure 6. Comparison of calculated and experimental results for a co-axial rotor in hovering flight.

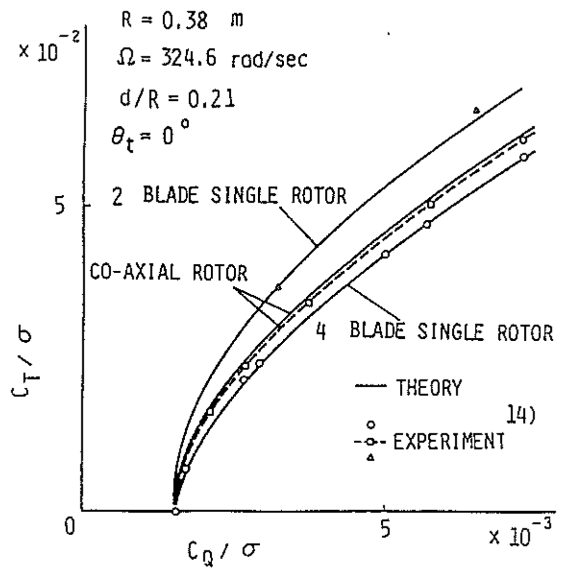

Figure 7. Comparison of calculated and experimental results for a co-axial rotor in hovering flight.

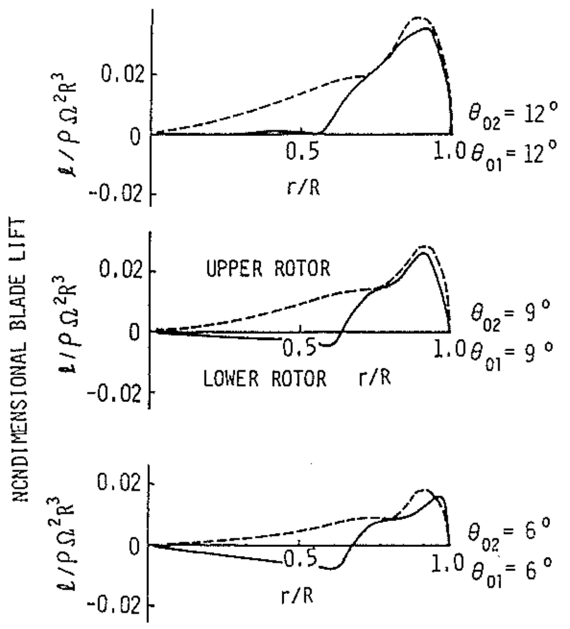

Figure 8. Calculated spanwise lift distribution in hover.

($d/R = 0.26$, $\theta_t = 0°$)

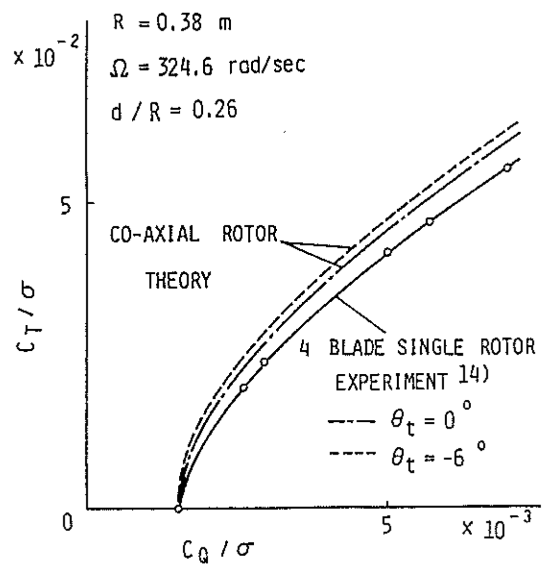

Figure 9. Effect of blade twist on co-axial rotor performance.

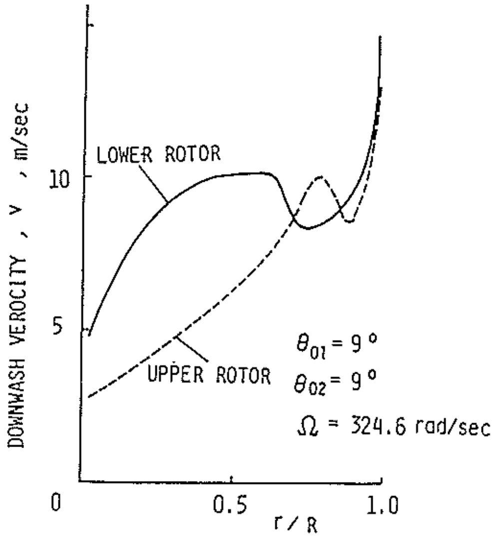

Figure 10. Induced downwash distribution.

($d/R = 0.26$, $\theta_t = 0°$)

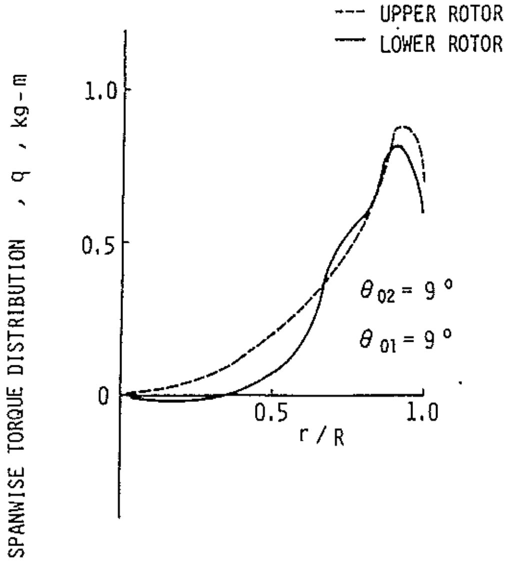

Figure 11. Example of spanwise torque distribution on a blade.

($d/R = 0.26$, $\theta_t = 0°$)

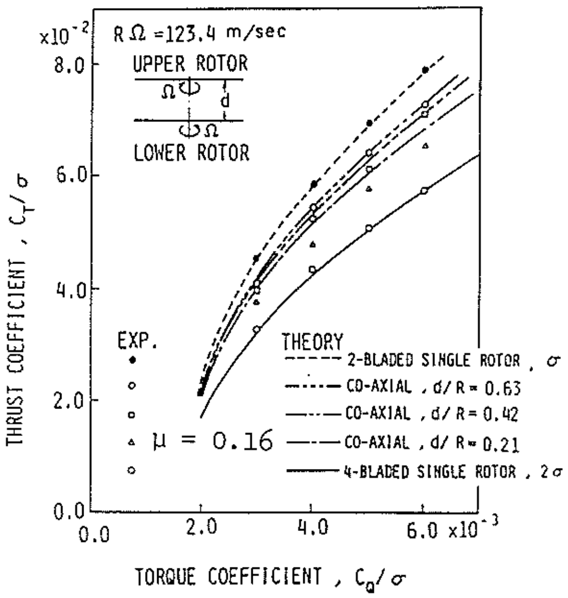

Figure 12. Polar curves for various rotor clearance.[8]

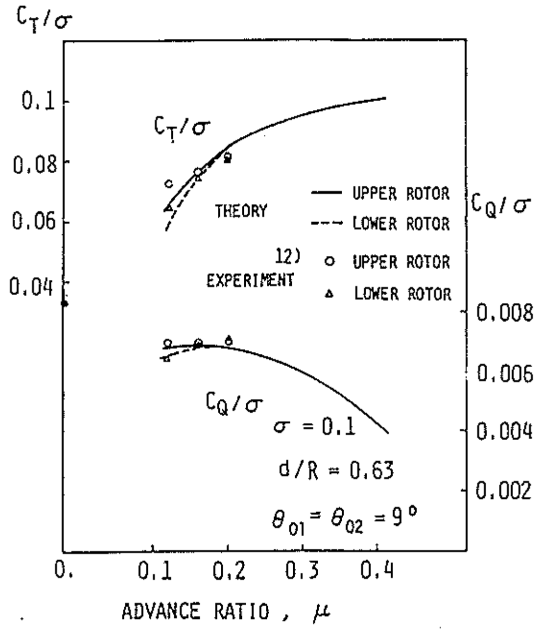

Figure 13. Aerodynamic characteristics of a co-axial rotor versus advance ratio.[8]

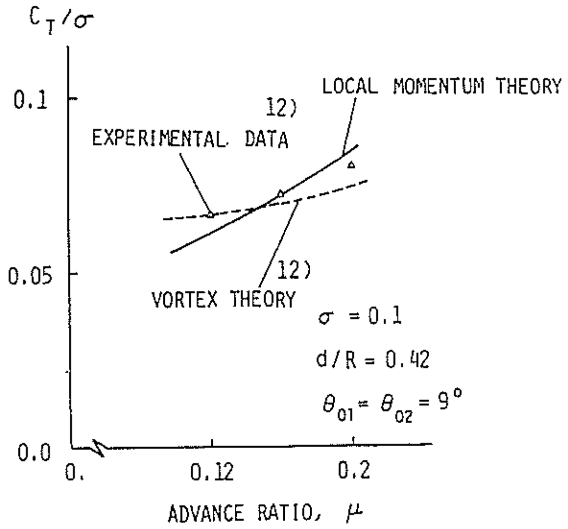

Figure 14. Blade loading characteristics of a co-axial rotor versus advance ratio.

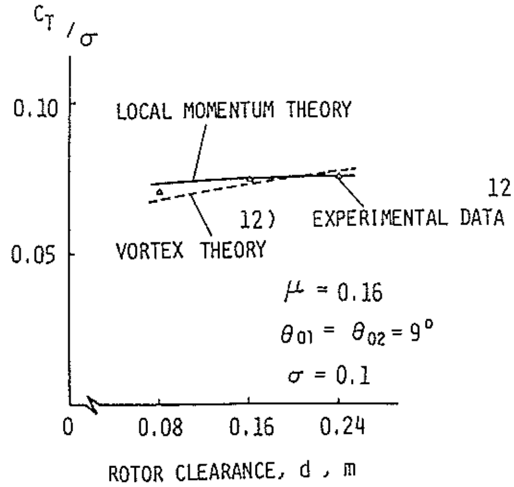

Figure 15. Blade loading characteristics of a co-axial rotor versus rotor clearance.

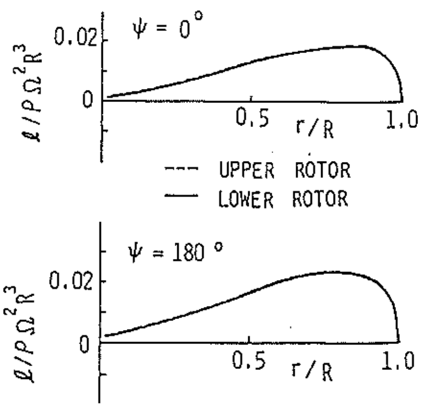

Figure 16. Calculated results of spanwise lift distribution in forward flight.

($d/R = 0.42$, $\theta_t = -6°$, $\mu = 0.16$, $\theta_{01} = \theta_{02} = 6°$)

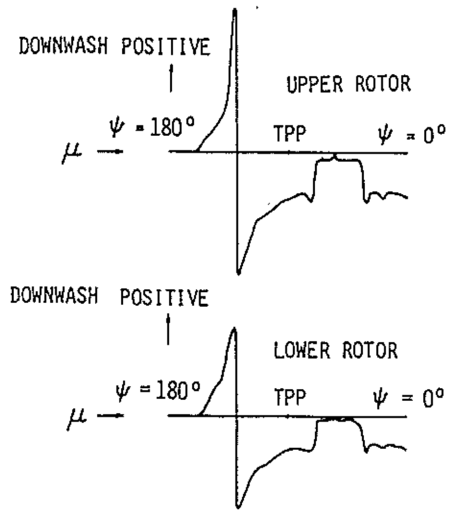

Figure 17. Downwash distribution on the rotor disc for a co-axial rotor in forward flight.

($\mu = 0.16$, $\theta_{01} = \theta_{02} = 6°$, $d/R = 0.42$, $\theta_t = -6°$)